PERGAMON

International Journal of Solids and Structures 40 (2003) 5649–5667

INTERNATIONAL JOURNAL OF SOLIDS and STRUCTURES

www.elsevier.com/locate/ijsolstr

Electrical nonlinear anti-plane shear crack in a functionally graded piezoelectric strip

Soon Man Kwon *

School of Mechanical Engineering, Yeungnam University, 214-1 Daedong, Kyongsan, Kyongbuk 712-749, South Korea

Received 26 March 2003; received in revised form 29 May 2003

Abstract

The electrical nonlinear behavior of an anti-plane shear crack in a functionally graded piezoelectric strip is studied by using the strip saturation model within the framework of linear electroelasticity. The analysis is conducted on the *electrically unified crack boundary condition* with the introduction of the electric crack condition parameter that can describe all the electric crack boundary condition in accordance with the aspect ratio of an ellipsoidal crack and the permittivity inside the crack, in particular, including traditional permeable and impermeable crack boundary conditions. The resulting mixed boundary value problem is analysed and near tip field is obtained by using the integral transform techniques. Numerical results for the normalized five kinds of energy release rates under the small scale electric saturation condition are presented and compared to show the influences of the electric crack condition parameter with the variation of the ellipsoidal crack parameters, electric loads, functionally graded piezoelectric material gradation, crack length, electromechanical coupling coefficient, and crack location. It reveals that there are considerable differences between the results obtained from the traditional electric crack models and those obtained from the current unified crack model.

Keywords: Functionally graded piezoelectric material; Unified crack boundary condition; Electric crack condition parameter; Energy release rate; Electrically saturated crack

1. Introduction

Now the main difficulty is remained ambiguous how to provide effective fracture criteria for piezoelectric materials. Two electrical crack boundary conditions have been commonly used to describing the fracture behavior in the piezoelectric materials; permeable and impermeable ones. An elliptic cavity in a piezoelectric material was considered by Zhang and Tong (1996) to study the boundary conditions on the cavity surface. In the limit, they found that the two commonly used boundary conditions are actually the two extreme cases of the exact boundary conditions. Of these extreme cases for the crack boundary conditions where permittivity of these cracks are assumed to be infinite and zero for a slit-like crack, respectively, the permeable assumption simply treats the crack as electrically conductive in which the applied electric loads

* Tel.: +82-53-810-2442; fax: +82-53-813-3703.
E-mail address: soonmankwon@hanmail.net (S.M. Kwon).

0020-7683/$ - see front matter © 2003 Elsevier Ltd. All rights reserved.
doi:10.1016/S0020-7683(03)00316-0

would contribute nothing to the fracture load, while the impermeable assumption considers the crack as electrically insulated in which the energy release rate (ERR) is always negative only in the presence of electric loading, irrespective of its sign. These contradict available experimental observations. Under applied mechanical and electrical loads, the crack will open or slide and there is an electrical potential difference between the upper and lower crack faces.

Motivated by some discrepancies between theory and experiment on fracture behavior of piezoelectric/ferroelectric materials, several important issues with the recognition of an essential role of the dielectric nonlinearity near the crack tip have been raised in the literature. In fact, piezoelectric crystals exhibit strong electrical nonlinearity at large field strength, Yang and Suo (1994), Lynch et al. (1995), Hao et al. (1996), Gong and Suo (1996), Ru et al. (1998) thought that polarization switching (domain wall switching) would occur near the crack tip under electromechanical loading, which would induce the spontaneous strain that has a great effect on the stress field. In order to derive a fracture criterion suitable for piezoelectrics, Gao and Barnett (1996), Gao et al. (1997) and Fulton and Gao (1997) adopted a multiscale viewpoint and identified a region of electrical nonlinearity near the crack tip in which the mechanical response of the material remains linear. This model can be considered as a generalization of the classical Dugdale model in fracture mechanics. They thought the piezoelectric ceramics can be considered as brittle materials and plastic yielding is rather difficult for these materials. But these materials are electrically more ductile. The plastic yielding zone ahead of the crack tip is much smaller than the electric saturation zone. Hence one should take into account of the effects of the electric saturation and neglect the effects of the plastic yielding. The *local* and *global* ERRs were derived by considering paths that pass and do not pass through the saturation strip, respectively. They found that the local ERR gives reasonable prediction with broadly agrees well with the experimental results. The local ERR indicates that the fracture stress is essentially a linear function of the applied electric field. However, the analysis given by Gao et al. (1997) is based on a simplified electroelasticity formulation. To overcome unproved the validity of their conclusions for a general poled ferroelectric, some researches (see Ru, 1999; Ru and Mao, 1999; Zhao et al., 1999; Wang, 2000; Shen et al., 2000) have presented a fully anisotropic analysis of the electric saturation model for piezoelectric materials. But, these approaches are based on the traditional either impermeable or permeable crack assumptions.

This paper is concerned with the problem for the electrically saturated crack in a functionally graded piezoelectric ceramic strip under the combined anti-plane shear and in-plane electrical loadings. The analysis has been conducted under the *electrically unified crack boundary condition* (Xu and Rajapakse, 2001; Wang and Mai, 2003) that can describe more reasonable cracks. The present unified crack model can express all of the permeable, impermeable and limited permeable crack boundary conditions by the introduction of the electric crack condition parameter (ECCP). Moreover, the proposed ECCP is derived in Section 4 in terms of two elliptic crack parameters, i.e. the ellipsoidal crack aspect ratio and the permittivity ratio inside a crack. It is assumed that the material properties of the functionally graded piezoelectric material vary smoothly according to an exponential function along the thickness of the strip. By using the integral transform techniques, the problem is first reduced to two pairs of dual integral equations and then into Fredholm integral equations of the second kind. Numerical results for the ERRs under small scale electric yielding condition are displayed graphically to show the influences of the ECCP considering the elliptic crack parameters, the electric loads, the functionally graded piezoelectric material gradation, the crack length, the electromechanical coupling coefficient (EMCC), and the crack location.

2. Problem statement and governing equations

Consider a crack of length $2a$ in a functionally graded piezoelectric strip, which is subjected to the combined mechanical and electric loads as shown in Fig. 1. A set of Cartesian coordinates (x, y, z) is

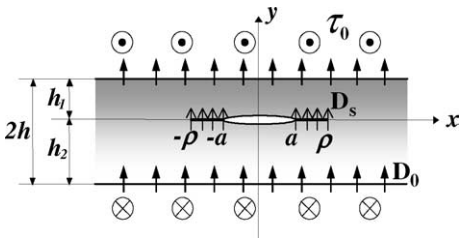

Fig. 1. Electrically saturated anti-plane shear crack in a functionally graded piezoelectric strip.

attached to the center of the crack for reference purposes, in which z-axis is not depicted. The functionally graded piezoelectric material of thickness $2h$, with z-axis being the poling direction, is thick enough in the z-direction to allow a state of anti-plane shear. The shear stress, τ_0, and electric displacement, D_0 are applied on the top and bottom surfaces. A strip electrical yielding model with electrical polarization reaching a saturation limit D_s is also prescribed along a line segment in front of the crack, $a \leqslant |x| < \rho$. For convenience, we assume that the functionally graded piezoelectric strip consists of upper (thickness h_1) and lower (thickness h_2) regions. Quantities in a functionally graded piezoelectric upper and lower layers will subsequently be designated by subscripts $i = 1$ and $i = 2$, respectively. Because of the assumed symmetry in geometry and loading, it is sufficient to consider the problem for $0 \leqslant x < \infty$ only.

In an anti-plane electroelastic boundary value problem, the constitutive relations for a functionally graded piezoelectric material in y-direction can be written as

$$\tau_{kzi}(x,y) = \mu(y)\frac{\partial w_i(x,y)}{\partial k} + e_{15}(y)\frac{\partial \psi_i(x,y)}{\partial k}, \quad D_{ki}(x,y) = -d_{11}(y)\frac{\partial \psi_i(x,y)}{\partial k} \qquad (k = x,y), \tag{1}$$

where

$$\psi_i(x,y) = \phi_i(x,y) - \frac{e_{15}(y)}{d_{11}(y)}w_i(x,y), \quad \mu(y) = c_{44}(y) + e_{15}^2(y)/d_{11}(y), \tag{2}$$

and τ_{kzi} and D_{ki} are the stress and electric displacement components, respectively. Also, w_i, ψ_i, ϕ_i, μ, d_{11}, c_{44} and e_{15} are the out-of-plane displacement components, the Bleustein function (Bleustein, 1968), the electric potential, the piezoelectrically stiffened elastic constant, the dielectric permittivity measured at a constant strain, the elastic shear modulus measured in a constant electric field and the piezoelectric constant, respectively.

To describe the effect of continuous composition gradient, Yamada et al. (2000) assumed that the variations in material constants, except the piezoelectric constant varying according to the exponential law (e.g. $e_{15} = e_{15}^0 \exp[\alpha(y/h - 1)]$), are not significant though the thickness, and thus are ignored. When a stepwise composition gradient or such Yamada-type gradients have been introduced in crack problem of functionally graded piezoelectric material, it increases the complexity of the problem significantly. In order to overcome the complexity of mathematics involved, however we will focus in this initial batch of studies on a special class of a functionally graded piezoelectric material in which the variations are in the same proportion (Jin and Zhong, 2002; Wang, 2003; Chen et al., 2003a,b). Therefore, we assume

$$c_{44}(y) = c_{44}^0 \exp(2\beta y), \quad e_{15}(y) = e_{15}^0 \exp(2\beta y), \quad d_{11}(y) = d_{11}^0 \exp(2\beta y). \tag{3}$$

Though the above assumption is unrealistic for all the material properties, however it would allow us to shed some light on the influence of the material gradient upon the stress and electric intensity factors.

Under the above consideration, the governing equations can be simplified to the following forms:

$$\nabla^2 w_i + 2\beta \frac{\partial w_i}{\partial y} = 0, \tag{4}$$

$$\nabla^2 \psi_i + 2\beta \frac{\partial \psi_i}{\partial y} = 0. \tag{5}$$

3. Solution to the problem

In order to obtain the desired electroelastic field, it is convenient to separate the problem considered into two sub-problems by the principle of superposition, one corresponding to the piezoelectric strip with no crack and the other corresponding to the piezoelectric strip with a crack for which the anti-plane shear stress and in-plane electric displacement applied at the crack surfaces are prescribed as the negative of those produced by the former, and the strip boundaries are also governed by appropriate conditions. From the viewpoint of fracture mechanics, of importance is the singular field disturbed by a crack. Consequently, one's attention is limited on the perturbation solution for a crack.

For a slit crack, since the dielectric constant of piezoceramic is much higher than that of the air (or vacuum) filling the crack, the electric boundary condition may be very sensitive to the crack opening or sliding caused by the applied mechanical and electric loads. Strictly, even if the permittivity of medium inside the crack is quite small, the flux of an electric field through the crack should not be zero. Hence, it is more reasonable to consider the electric field inside the crack and the electric jump across the crack simultaneously. In this case, the crack can be modeled as a dielectric crack filled with a dielectric medium, i.e. limited permeable crack. To this end, we prescribe D_y^c as the normal component of the electric displacement on the crack surfaces (Xu and Rajapakse, 2001; Wang and Mai, 2003). For convenience of analysis, we introduce a newly defined ECCP as $D_r = D_y^c/D_0$. D_r is zero for an *impermeable* crack, $(D_r)_{\text{perm}}$ for a *permeable* crack to be determined in Section 4, and unknown for a *limited permeable* crack. It also depends on the aspect ratio of an elliptic crack and the permittivity inside a crack, of which the relation with the ellipsoidal crack parameters will be determined in Section 4 and will be presented graphically in Section 5.

By the principle of superposition, the boundary conditions on the cracked plane $y = 0$ can be described as follows:

$$\tau_{yzi}(x,0) = -\tau_0 \quad (0 \leqslant x < a), \tag{6}$$

$$w_1(x,0) = w_2(x,0) \quad (a \leqslant x < \infty), \tag{7}$$

$$D_{yi}(x,0) = -D_0(1 - D_r) + D_s H(x-a) \quad (0 \leqslant x < \rho), \tag{8}$$

$$\phi_1(x,0) = \phi_2(x,0) \quad (\rho \leqslant x < \infty), \tag{9}$$

in which $H(x-a)$ is the Heaviside unit step function. Eqs. (8) and (9) will be referred to hereafter electrically "*unified*" (or "*natural*" in Wang and Mai (2003)) crack boundary condition. The solution to be presented here will correctly recover both the impermeable and permeable crack solutions as limiting solutions later (Section 4.1).

On the $y = h_1$, $y = -h_2$, and $y = 0$, the boundary conditions are written as follows:

$$\tau_{yz1}(x,h_1) = \tau_{yz2}(x,-h_2) = 0, \tag{10}$$

$$D_{y1}(x,h_1) = D_{y2}(x,-h_2) = 0, \tag{11}$$

$$\tau_{yz1}(x,0) = \tau_{yz2}(x,0) \quad (a \leqslant x < \infty), \tag{12}$$

$$D_{y1}(x,0) = D_{y2}(x,0) \quad (a \leqslant x < \infty). \tag{13}$$

To solve the problem stated above, it is convenient to employ an integral transform technique to reduce the associated mixed boundary value problem to dual integral equations. For this purpose, by use of the Fourier cosine transform, let the solutions of Eqs. (4) and (5) be given by

$$w_i(x,y) = \frac{2}{\pi}\int_0^\infty [A_{1i}(s)e^{p_1 y} + A_{2i}(s)e^{p_2 y}]\cos(sx)\,ds, \tag{14}$$

$$\psi_i(x,y) = \frac{2}{\pi}\int_0^\infty [B_{1i}(s)e^{p_1 y} + B_{2i}(s)e^{p_2 y}]\cos(sx)\,ds, \tag{15}$$

where

$$p_1 = -\beta + \sqrt{s^2+\beta^2}, \quad p_2 = -\beta - \sqrt{s^2+\beta^2}, \tag{16}$$

and $A_{ki}(s)$ and $B_{ki}(s)$ $(i,k = 1,2)$ are the unknowns to be solved.

With the aid of constitutive equation (1), it follows that the electric potential $\phi_i(x,y)$, the components of the stress $\tau_{yzi}(x,y)$ and the electric displacements $D_{yi}(x,y)$ are given by

$$\phi_i(x,y) = \frac{e_{15}^0}{d_{11}^0}\frac{2}{\pi}\int_0^\infty [A_{1i}(s)e^{p_1 y} + A_{2i}(s)e^{p_2 y}]\cos(sx)\,ds + \frac{2}{\pi}\int_0^\infty [B_{1i}(s)e^{p_1 y} + B_{2i}(s)e^{p_2 y}]\cos(sx)\,ds, \tag{17}$$

$$\begin{aligned}\tau_{yzi}(x,y) = {} & \frac{2\mu_0 e^{2\beta y}}{\pi}\int_0^\infty [p_1 A_{1i}(s)e^{p_1 y} + p_2 A_{2i}(s)e^{p_2 y}]\cos(sx)\,ds \\ & + \frac{2e_{15}^0 e^{2\beta y}}{\pi}\int_0^\infty [p_1 B_{1i}(s)e^{p_1 y} + p_2 B_{2i}(s)e^{p_2 y}]\cos(sx)\,ds,\end{aligned} \tag{18}$$

$$D_{yi}(x,y) = -\frac{2d_{11}^0 e^{2\beta y}}{\pi}\int_0^\infty [p_1 B_{1i}(s)e^{p_1 y} + p_2 B_{2i}(s)e^{p_2 y}]\cos(sx)\,ds, \tag{19}$$

with

$$\mu_0 = c_{44}^0 + \frac{(e_{15}^0)^2}{d_{11}^0}. \tag{20}$$

It is convenient to introduce the unknown two functions $P_1(s)$ and $P_2(s)$ by substituting Eqs. (18) and (19) into Eqs. (12) and (13), respectively:

$$p_1[A_{11}(s) - A_{12}(s)] = -p_2[A_{21}(s) - A_{22}(s)] \equiv \frac{2p_1 p_2}{p_2 - p_1}P_1(s), \tag{21}$$

$$p_1[B_{11}(s) - B_{12}(s)] = -p_2[B_{21}(s) - B_{22}(s)] \equiv \frac{2p_1 p_2}{p_2 - p_1}P_2(s). \tag{22}$$

Using the above results, in conjunction with the continuity conditions (10) and (11) we find:

$$A_{11}(s) = -\frac{2p_2^2}{p_2 - p_1}e^{(p_2 - p_1)h_1}R_1(s)P_1(s), \tag{23}$$

$$A_{21}(s) = -\frac{2p_1p_2}{p_2 - p_1}R_1(s)P_1(s), \tag{24}$$

$$A_{12}(s) = A_{11}(s) - \frac{2p_2}{p_2 - p_1}P_1(s), \tag{25}$$

$$A_{22}(s) = -\frac{p_1}{p_2}e^{(p_2-p_1)h_2}A_{12}(s), \tag{26}$$

$$B_{11}(s) = -\frac{2p_2^2}{p_2 - p_1}e^{(p_2-p_1)h_1}R_1(s)P_2(s), \tag{27}$$

$$B_{21}(s) = -\frac{2p_1p_2}{p_2 - p_1}R_1(s)P_2(s), \tag{28}$$

$$B_{12}(s) = B_{11}(s) - \frac{2p_2}{p_2 - p_1}P_2(s), \tag{29}$$

$$B_{22}(s) = -\frac{p_1}{p_2}e^{(p_2-p_1)h_2}B_{12}(s), \tag{30}$$

in which

$$R_1(s) = \frac{1}{p_2}\left[\frac{1 - e^{(p_2-p_1)h_2}}{1 - e^{(p_2-p_1)(h_1+h_2)}}\right]. \tag{31}$$

Substituting the above relationships into the remaining two mixed boundary conditions of Eqs. (6)–(9), it leads to the following two simultaneous dual integral equations:

$$\int_0^\infty sF(s)[\mu_0P_1(s) + e_{15}^0P_2(s)]\cos(sx)\,ds = \frac{\pi}{2}\tau_0 \quad (0 \leqslant x < a), \tag{32}$$

$$\int_0^\infty P_1(s)\cos(sx)\,ds = 0 \quad (a \leqslant x < \infty), \tag{33}$$

$$\int_0^\infty sF(s)P_2(s)\cos(sx)\,ds = -\frac{\pi D_0}{2d_{11}^0}\left[(1 - D_r) - \frac{D_s}{D_0}H(x-a)\right] \quad (0 \leqslant x < \rho), \tag{34}$$

$$\int_0^\infty \left[\frac{e_{15}^0}{d_{11}^0}P_1(s) + P_2(s)\right]\cos(sx)\,ds = 0 \quad (\rho \leqslant x < \infty), \tag{35}$$

where

$$\begin{aligned} F(s) &= \frac{s}{\sqrt{s^2+\beta^2}}\frac{2}{\coth\left(\sqrt{s^2+\beta^2}h_1\right) + \coth\left(\sqrt{s^2+\beta^2}h_2\right)} \\ &= \frac{s}{\sqrt{s^2+\beta^2}}\left[\tanh\left(\sqrt{s^2+\beta^2}h\right) - \frac{2\sinh^2\left(\sqrt{s^2+\beta^2}e\right)}{\sinh\left(2\sqrt{s^2+\beta^2}h\right)}\right], \end{aligned} \tag{36}$$

$$e = h - h_1 = h_2 - h. \tag{37}$$

Next, the solutions of the dual integral equations (32)–(35) can be attempted by using well-known techniques, outlined in Copson (1961). That is, we choose $P_1(s)$ and $P_2(s)$ in terms of auxiliary functions $\Omega_1(\xi)$ and $\Omega_2(\xi)$, respectively, given in the forms:

$$P_1(s) = \frac{\pi a^2}{2\mu_0}\tau_0(1+\Lambda_0)\int_0^1 \sqrt{\xi}\Omega_1(\xi)J_0(sa\xi)\,\mathrm{d}\xi, \tag{38}$$

$$P_2(s) = -\frac{\pi\rho^2}{2}\frac{D_0(1-D_r)}{d_{11}^0}\int_0^1 \sqrt{\xi}\Omega_2(\xi)J_0(s\rho\xi)\,\mathrm{d}\xi, \tag{39}$$

where

$$\Lambda_0 = \lambda_0(1-D_r); \quad \lambda_0 = \frac{e_{15}^0}{d_{11}^0}\frac{D_0}{\tau_0}, \tag{40}$$

and $J_0(\cdot)$ stands for the zero-order Bessel function of the first kind.

Applying Eqs. (38) and (39) into Eqs. (32)–(35), it is easily shown that Eqs. (33) and (35) are automatically satisfied, and Eqs. (32) and (34) yield Fredholm integral equations of the second kind:

$$\Omega_1(\xi) + \int_0^1 \Omega_1(\eta)L_1(\xi,\eta)\,\mathrm{d}\eta = \sqrt{\xi}, \tag{41}$$

$$\Omega_2(\xi) + \int_0^1 \Omega_2(\eta)L_2(\xi,\eta)\,\mathrm{d}\eta = \sqrt{\xi}M_2(\xi), \tag{42}$$

where

$$L_1(\xi,\eta) = \sqrt{\xi\eta}\int_0^\infty s[F(s/a)-1]J_0(s\xi)J_0(s\eta)\,\mathrm{d}s, \tag{43}$$

$$L_2(\xi,\eta) = \sqrt{\xi\eta}\int_0^\infty s[F(s/\rho)-1]J_0(s\xi)J_0(s\eta)\,\mathrm{d}s, \tag{44}$$

$$M_2(\xi) = \begin{cases} 1 & \left(\xi < \dfrac{a}{\rho}\right), \\ 1 - \dfrac{2}{\pi}\dfrac{D_s}{D_0}\dfrac{\cos^{-1}\left(\dfrac{a/\rho}{\xi}\right)}{1-D_r} & \left(\dfrac{a}{\rho} \leqslant \xi < 1\right). \end{cases} \tag{45}$$

4. Intensity factors and ERR

To find the asymptotic fields in the neighborhood of the crack tip, the portions of $P_1(s)$ and $P_2(s)$ that contribute to the singular behaviors are found from the integration of Eqs. (38) and (39) by parts in the forms:

$$P_1(s) = \frac{\pi\tau_0(1+\Lambda_0)a}{2\mu_0}\frac{1}{s}\left\{\Omega_1(1)J_1(sa) - \int_0^1 \xi J_1(sa\xi)\frac{\mathrm{d}}{\mathrm{d}\xi}\left[\frac{\Omega_1(\xi)}{\sqrt{\xi}}\right]\mathrm{d}\xi\right\}, \tag{46}$$

$$P_2(s) = -\frac{\pi D_0(1-D_r)\rho}{2d_{11}^0}\frac{1}{s}\left\{\Omega_2(1)J_1(s\rho) - \int_0^1 \xi J_1(s\rho\xi)\frac{\mathrm{d}}{\mathrm{d}\xi}\left[\frac{\Omega_2(\xi)}{\sqrt{\xi}}\right]\mathrm{d}\xi\right\}, \tag{47}$$

where $J_1(\cdot)$ denotes the first-order Bessel function of the first kind. The integrals in Eqs. (46) and (47) are bounded at $x = \pm a$ and $x = \pm\rho$, respectively. Thus the singular behaviors of the stress and electric fields are governed by the leading terms containing $\Omega_1(1)$ and $\Omega_2(1)$, respectively.

From the above results, after some lengthy algebra the singular parts of the stresses, strain, electric displacement, and electric fields in the neighborhood of the crack tip can be expressed as

$$\tau_{xz} = -\frac{K_{\mathrm{III}}}{\sqrt{2\pi r}}\sin\left(\frac{\theta}{2}\right), \quad \tau_{yz} = \frac{K_{\mathrm{III}}}{\sqrt{2\pi r}}\cos\left(\frac{\theta}{2}\right), \tag{48}$$

$$\gamma_{xz} = \frac{\partial w}{\partial x} = -\frac{K^{\gamma}}{\sqrt{2\pi r}}\sin\left(\frac{\theta}{2}\right), \quad \gamma_{yz} = \frac{\partial w}{\partial y} = \frac{K^{\gamma}}{\sqrt{2\pi r}}\cos\left(\frac{\theta}{2}\right), \tag{49}$$

$$D_x = -\frac{K^{\mathrm{D}}}{\sqrt{2\pi r_1}}\sin\left(\frac{\theta_1}{2}\right), \quad D_y = \frac{K^{\mathrm{D}}}{\sqrt{2\pi r_1}}\cos\left(\frac{\theta_1}{2}\right), \tag{50}$$

$$E_x = -\frac{\partial\phi}{\partial x} = -\frac{K^{\mathrm{E}}}{\sqrt{2\pi r_1}}\sin\left(\frac{\theta_1}{2}\right), \quad E_y = -\frac{\partial\phi}{\partial y} = \frac{K^{\mathrm{E}}}{\sqrt{2\pi r_1}}\cos\left(\frac{\theta_1}{2}\right), \tag{51}$$

where

$$r = \sqrt{(x-a)^2 + y^2}, \quad \theta = \tan^{-1}\left(\frac{y}{x-a}\right), \tag{52}$$

$$r_1 = \sqrt{(x-\rho)^2 + y^2}, \quad \theta_1 = \tan^{-1}\left(\frac{y}{x-\rho}\right). \tag{53}$$

Also K_{III}, K^{γ}, K^{D} and K^{E} are the stress intensity factor (SIF), the strain intensity factor, the electric displacement intensity factor, and the electric field intensity factor, respectively. These field intensity factors are given by

$$K_{\mathrm{III}} = \lim_{x\to a^+}\sqrt{2\pi(x-a)}\tau_{yzi}(x,0) = \tau_0(1+\Lambda_0)\sqrt{\pi a}\Omega_1(1), \tag{54}$$

$$K^{\gamma} = \lim_{x\to a^+}\sqrt{2\pi(x-a)}\gamma_{yzi}(x,0) = \frac{K_{\mathrm{III}}}{c_{44}^0(1+k_0^2)} = \frac{K_{\mathrm{III}}}{\mu_0}, \tag{55}$$

$$K^{\mathrm{D}} = \lim_{x\to\rho^+}\sqrt{2\pi(x-\rho)}D_{yi}(x,0) = D_0(1-D_r)\sqrt{\pi\rho}\Omega_2(1) = \frac{e_{15}^0}{c_{44}^0}\frac{\Lambda_0}{k_0^2}\tau_0\sqrt{\pi\rho}\Omega_2(1), \tag{56}$$

$$K^{\mathrm{E}} = \lim_{x\to\rho^+}\sqrt{2\pi(x-\rho)}E_{yi}(x,0) = \frac{K^{\mathrm{D}}}{d_{11}^0}, \tag{57}$$

in which the parameter k_0 is a measure of the strength of the electromechanical coupling in a piezoelectric solid which is related with the electroacoustic surface wave (i.e. Bleustein–Gulyaev wave), and was introduced as the EMCC in Kwon et al. (2002a,b) given by

$$k_0 = \sqrt{(e_{15}^0)^2/c_{44}^0 d_{11}^0}. \tag{58}$$

It should be noted in Eq. (54) that the SIF based on the unified electric crack condition casts a clue on the effect of electric load, which is different from that of traditional approaches. Thus it can be predicted by the SIF that the crack growth is promoted or inhibited the crack growth depending the direction of electric loads.

Since the electric displacement and the electric field at the physical crack tip are finite, the singularity must vanish. As a result,

$$K^{\mathrm{D}} = K^{\mathrm{E}} = 0. \tag{59}$$

This requirement is used to determine the equilibrium length, $\omega_s = \rho - a$, of the electrically yielded zone.

$$\frac{\omega_s}{a} = \sec\left\{\frac{\pi}{2}\frac{D_0}{D_s}(1 - D_r)[1 - P(\rho/h)]\right\} - 1, \tag{60}$$

where

$$P(\rho/h) = \int_0^1 L_2(1,\eta)\Omega_2(\eta)\,\mathrm{d}\eta. \tag{61}$$

Expanding the resultant secant function of Eq. (60) in series form, we find that, for $D_0/D_s \ll 1$,

$$\omega_s \approx \frac{\pi^2 a}{8}\left\{\frac{D_0}{D_s}(1 - D_r)[1 - P(\rho/h)]\right\}^2. \tag{62}$$

To evaluate the ERR of piezoelectric materials, we use the J-integral (Cherrepanov, 1979) as

$$J = \int_\Gamma \left(Hn_1 - \tau_{ij}n_j u_{i,1} + D_i n_i E_1\right)\mathrm{d}\Gamma, \tag{63}$$

where H is the electric enthalpy per unit volume that satisfies $\partial H/\partial\gamma_{ij} = \tau_{ij}$ and $\partial H/\partial E_i = -D_i$, n_i is the unit outward normal component along the path Γ.

Two ERRs emerge from this problem as in Gao et al. (1997). Near the crack tip ($a \leqslant x < \rho$), the fields are mechanically singular and electrically nonsingular. The local ERR corresponding to J-integral along an infinitesimal local contour Γ_c (Fig. 2) is

$$G_c = \frac{K_{\mathrm{III}}K^{\gamma}}{2} = \frac{K_{\mathrm{III}}^2}{2\mu_0} = \frac{\tau_0^2\pi a(1 + \Lambda_0)^2}{2c_{44}^0(1 + k_0^2)}\Omega_1^2(1), \tag{64}$$

where G_c is a *local* ERR.

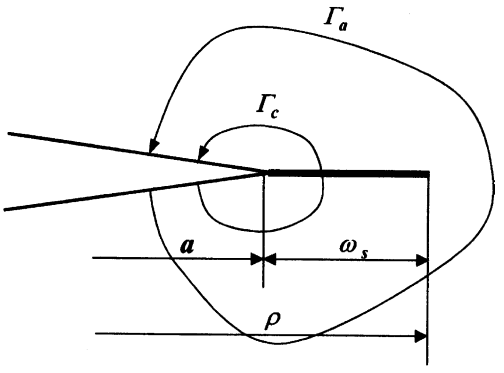

Fig. 2. J-integral contours for evaluating local and global ERRs.

It should be stated that the local ERR is always positive, i.e. $G_c \geqslant 0$. Also we can confirm that the relationship between the local ERR and the SIF is consistent with that of conventional purely elastic fracture mechanics.

Another ERR can be obtained by evaluating J-integral along a global contour Γ_a shown in Fig. 2. Using the path-independent property of J-integral, the contour Γ_a can be deformed to follow the electrical yielding zone and join with the local contour Γ_c at the crack tip. When this is done, the apparent (or *global*) ERR is found to be

$$G_a = \frac{K_{\mathrm{III}}K^{\gamma} - K^{\mathrm{D}}K^{\mathrm{E}}}{2} = G_c - \frac{D_0^2\pi\rho(1-D_r)^2}{2d_{11}^0}\Omega_2^2(1). \tag{65}$$

If a fracture criterion based on G_a were used, we would predict that the electric load should inhibit crack growth irrespective of its sign. This is contradictory to the experimental results. On the other hand, a fracture criterion based on G_c would predict that fracture is promoted by a positively applied electric load and inhibited by a negatively applied electric field. Han and Wang (1999) stated that the electric saturation zone size or strip length in the saturation strip model remains unchanged during the crack propagation and thus only the mechanical energy is taking into account in the local ERR. In this sense, the local ERR provides a physical basis for the mechanical ERR of Park and Sun (1995) hard to justify physically (McMeeking, 1999).

When the size of the saturated strip is vanishingly small, i.e. $\omega_s \ll a$ and $\Omega_2(1) \to \Omega_1(1)$, it follows from Eq. (65) that

$$(G_a)_{\mathrm{SSY}} = G_a(\rho \to a) = \frac{\tau_0^2\pi a}{2c_{44}^0}\left[\frac{(1+\Lambda_0)^2}{1+k_0^2} - \frac{\Lambda_0^2}{k_0^2}\right]\Omega_1^2(1). \tag{66}$$

4.1. Traditional crack solutions

In what follows, we consider two special cases, viz. the impermeable crack and the permeable crack. First, if the ECCP $D_r = 0$ (or $\Lambda_0 = \lambda_0$) under the consideration of the small scale electric yielding condition, then the solutions of the impermeable crack are written as

$$K_{\mathrm{III}} = \tau_0(1+\lambda_0)\sqrt{\pi a}\Omega_1(1), \tag{67}$$

$$K^{\mathrm{D}} = D_0\sqrt{\pi a}\Omega_2(1) = \frac{e_{15}^0}{c_{44}^0}\frac{\lambda_0}{k_0^2}\tau_0\sqrt{\pi a}\Omega_2(1), \tag{68}$$

$$G_c = \frac{\tau_0^2\pi a(1+\lambda_0)^2}{2c_{44}^0(1+k_0^2)}\Omega_1^2(1), \tag{69}$$

$$(G_a)_{\mathrm{SSY}} = \frac{\tau_0^2\pi a}{2c_{44}^0}\left[\frac{(1+\lambda_0)^2}{1+k_0^2} - \frac{\lambda_0^2}{k_0^2}\right]\Omega_1^2(1). \tag{70}$$

It is found that Eqs. (68) and (70) are in exact agreement with the forms of the traditional impermeable approaches, but the SIF of Eq. (67) is not consistent with that of the traditional impermeable approach. Next, to find the ECCP D_r satisfying the permeable assumption it needs an additional condition as follows:

$$\begin{aligned} &E_{x1}(x,0^+) = E_{x2}(x,0^-) \quad (0 \leqslant x < a) \\ &(\text{or equivalently } \phi_1(x,0^+) = \phi_2(x,0^-) \quad (0 \leqslant x < a)). \end{aligned} \tag{71}$$

It gives

$$(D_r)_{\text{perm}} = 1 - \chi(\rho)\frac{k_0^2}{\lambda_0}, \tag{72}$$

where

$$\chi(\rho) = \left[(1+k_0^2)\frac{\Omega_2(1)}{\Omega_1(1)}\sqrt{\frac{a^2-x^2}{\rho^2-x^2}} - k_0^2\right]^{-1}. \tag{73}$$

It should be noted that $\chi \to 1$ when the size of the saturated strip is very small. Therefore, if we consider $D_r = (D_r)_{\text{perm}}$ with the condition of $\chi \to 1$, i.e. $\Lambda_0 = k_0^2$:

$$K_{\text{III}} = \tau_0(1+k_0^2)\sqrt{\pi a}\Omega_1(1), \tag{74}$$

$$K^{\text{D}} = D_0\frac{k_0^2}{\lambda_0}\sqrt{\pi a}\Omega_2(1) = \frac{e_{15}^0}{c_{44}^0}\tau_0\sqrt{\pi a}\Omega_2(1), \tag{75}$$

$$G_c = \frac{\tau_0^2\pi a(1+k_0^2)}{2c_{44}^0}\Omega_1^2(1), \tag{76}$$

$$(G_a)_{\text{SSY}} = \frac{\tau_0^2\pi a}{2c_{44}^0}\Omega_1^2(1). \tag{77}$$

The similar trend on the SIF as in an impermeable crack is also observed in the above permeable crack.

It must be addressed that the ECCP can be associated with two parameters in an elliptical flaw, i.e. the permittivity ratio and the crack aspect ratio. The permittivity ratio κ and the aspect ratio α are defined as $\kappa = d_{11}^0/\varepsilon_a$ (d_{11}^0 and ε_a are dielectric permittivity of the ceramic and ellipse interior) and $\alpha = a/b$ (a and b are the major and minor axes of the ellipse). From the well-established result of Zhang and Tong (1996), we can determine the ECCP for an elliptical flaw of the form:

$$D_r = \frac{1+(1/\alpha)}{1+(1+k_0^2)(\kappa/\alpha)}(D_r)_{\text{perm}}. \tag{78}$$

From the above, reconsider a mathematically slit-like crack ($\alpha \to \infty$). In the case, there are three limits:

(i) $D_r = (D_r)_{\text{perm}}$ for a *permeable* crack when $\kappa/\alpha \to 0$ (or $\varepsilon_a \to \infty$),
(ii) $D_r = \frac{1}{1+(1+k_0^2)(\kappa/\alpha)}(D_r)_{\text{perm}}$ for a *limited permeable* crack when $\kappa/\alpha \to$ constant,
(iii) $D_r \to 0$ for an *impermeable* crack when $\kappa/\alpha \to \infty$ (or $\varepsilon_a \to 0$).

Hence, the traditional impermeable and permeable crack boundary conditions are actually the two extremes of the unified crack boundary condition.

5. Numerical results and discussion

In this section, the dependences of ERRs under small scale electric yielding condition upon the ECCP, the electric loads, the material gradient, the EMCC, and the crack geometry are examined. From the viewpoint of experiment, it is much simpler to measure or impose the potential difference between two surfaces of the piezoelectric material than the charge. For this goal, an electrical to mechanical load ratio,

$\zeta_0 = e_{15}^0 E_0/\tau_0$ is introduced. The relationship between normalized electric loads λ_0 and ζ_0 in a functionally graded piezoelectric strip can be found from the constitutive equation (1) as

$$\lambda_0 = k_0^2 + e^{2\beta h_1}(1+k_0^2)\zeta_0, \quad \text{or} \quad \zeta_0 = \frac{e_{15}^0 E_0}{\tau_0} = \frac{\lambda_0 - k_0^2}{e^{2\beta h_1}(1+k_0^2)}. \tag{79}$$

We also introduce the following normalized ERRs to clarify the differences between the selected electrical crack conditions:

$$G_c^* = \frac{G_c}{G_{\text{ref}}} = \frac{(1+\Lambda_0)^2}{1+k_0^2}\Omega_1^2(1) \quad \text{(saturated unified crack)} \tag{80}$$

$$G_i^* = \left[\frac{G_c}{G_{\text{ref}}}\right]_{D_r=0} = \frac{(1+\lambda_0)^2}{1+k_0^2}\Omega_1^2(1) \quad \text{(saturated impermeable crack)} \tag{81}$$

$$G_p^* = \left[\frac{G_c}{G_{\text{ref}}}\right]_{D_r=(D_r)_{\text{perm}}} = (1+k_0^2)\Omega_1^2(1) \quad \text{(saturated permeable crack)} \tag{82}$$

$$(G_i^*)_{\text{SSY}} = \left[\frac{(G_a)_{\text{SSY}}}{G_{\text{ref}}}\right]_{D_r=0} = \left[\frac{(1+\lambda_0)^2}{1+k_0^2} - \frac{\lambda_0^2}{k_0^2}\right]\Omega_1^2(1) \quad \text{(traditional impermeable crack)} \tag{83}$$

$$(G_p^*)_{\text{SSY}} = \left[\frac{(G_a)_{\text{SSY}}}{G_{\text{ref}}}\right]_{D_r=(D_r)_{\text{perm}}} = \Omega_1^2(1) \quad \text{(traditional permeable crack)} \tag{84}$$

where $G_{\text{ref}} = (\tau_0^2\pi a)/(2c_{44}^0)$.

Fig. 3 depicts the local ERR G_c^* in accordance with the ECCP D_r at $\zeta_0 = \pm 0.2$. The local ERR G_c^* decrease with the increase of D_r. It is observed that under the positive electric loading G_i^* is larger than G_p^*, but the trend is reversed under the negative one.

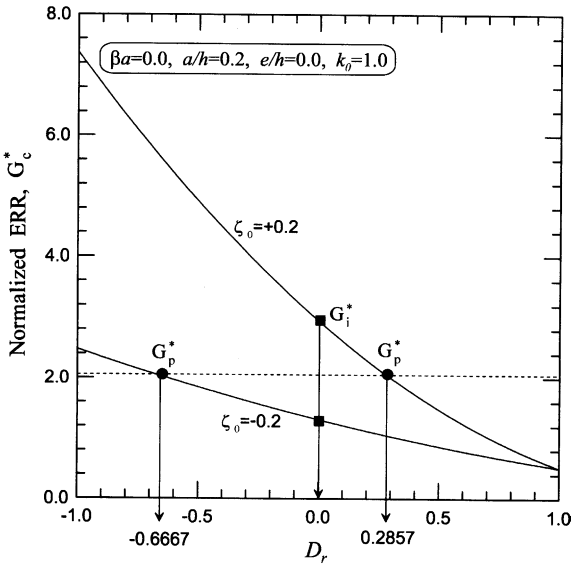

Fig. 3. Normalized ERR G_c^* versus the electrical crack condition parameter D_r in a center cracked piezoelectric strip.

In Figs. 4 and 5, the influences of the aspect ratio of an elliptic crack and the permittivity inside a crack on the local ERR are displayed. In Fig. 4, the local ERR for an elliptical flaw with an aspect ratio $\alpha = 100$ is computed with the variation of κ. The computational results shows that the effects on the local ERR are more salient in the small range of κ and under larger electric fields.

In Fig. 5, a computation is performed with $\kappa = 1000$, which is the order of the permittivity ratio of a ferroelectric ceramic to that of free surface. Flaws are varied in the range of $\alpha \leqslant 1000$. The ERRs decrease

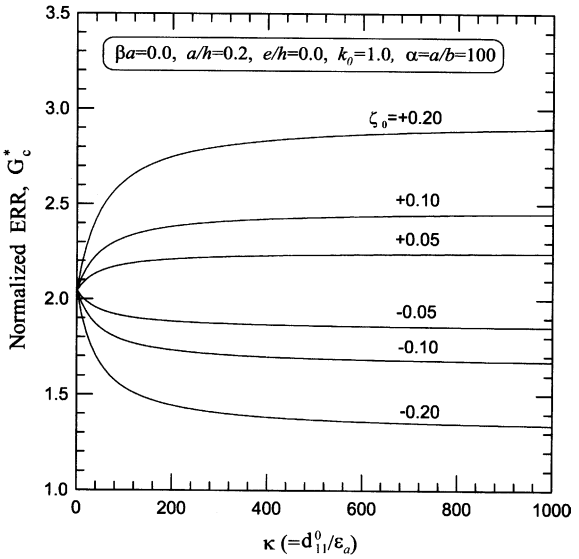

Fig. 4. Comparison of G_c^* of elliptic flaws with different permittivity ratios of κ in a center cracked piezoelectric strip.

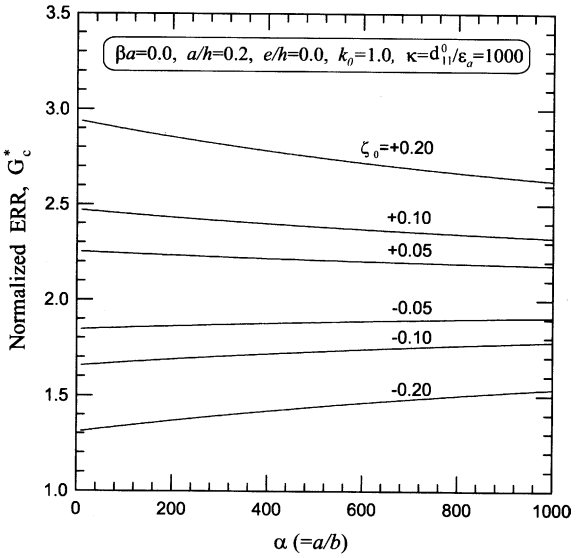

Fig. 5. Comparison of G_c^* of elliptic flaws with different aspect ratios of α in a center cracked piezoelectric strip.

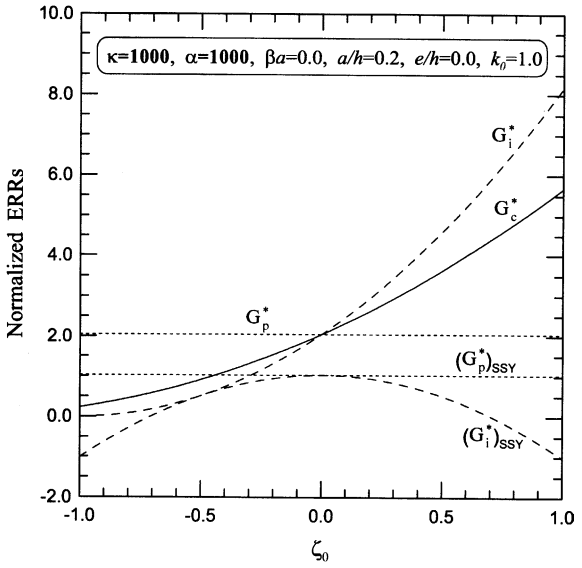

Fig. 6. Normalized ERRs versus ζ_0 in a center cracked piezoelectric strip.

or increase depending on the direction of electric field as the aspect ratio increase. The effect of aspect ratio is smaller as the electric fields are smaller.

Fig. 6 displays the dependence of the electric fields ζ_0 on the normalized ERRs in an ellipsoidal flaw of $\kappa = 1000$ and $\alpha = 1000$. It is observed firstly that the crack based on the local ERRs will never close and this is the actual case. Remarkable another observation is that the solution based on the unified crack boundary condition falls between those obtained from the impermeable crack and permeable crack. That is, G_i^* may be prone to overestimate and G_p^* underestimate the real crack under the positive electric fields, whereas the trend is opposite under the negative electric fields. On the while the permeable assumption is considered, no electric field concentration occurs, and the electric field makes no contribution to the ERR. The local ERRs G_c^* and G_i^* always increase with the increase of ζ_0 irrespective of the direction of electric field. This means that the crack growth is promoted under the positive electric field, while retarded under the negative one. Also the well-known traditional ERR $(G_i^*)_{\mathrm{SSY}}$ does not give an explanation for the crack growth on the direction of electric field. Because $(G_i^*)_{\mathrm{SSY}}$ at higher electric loads are negative irrespective of the direction of electric field.

Fig. 7(a) and (b) show the effect of material gradation βa on the normalized local ERRs under the uniform electric displacements and the uniform electric fields, respectively. Under the constant electric displacement (Fig. 7(a)) all the local ERRs have the symmetric property with respect to $\beta a = 0$, and those decrease or increase depending on the sign and magnitude of βa. It should be stated under the uniform electric displacement that the local ERRs of the functionally graded piezoelectric ceramic are higher than those of homogeneous piezoelectric materials ($\beta a = 0$). Though the local ERRs in the functionally graded piezoelectric ceramic are increased, this deleterious effect will be completely offset by the high fracture toughness of the functionally graded piezoelectric ceramic as in a purely elastic problem (Jin and Batra, 1996) and as a result, the residual strength of the cracked functionally graded piezoelectric ceramic will be much higher than that of the homogeneous piezoelectric ceramic. On the other hand, the trend under the constant electric field (Fig. 7(b)) is different that of constant electric displacement. The trend in the local ERR G_p^* based on the permeable assumption is exactly the same as that of the constant electric displacement, however, the local ERRs G_c^* and G_i^* firstly decrease and reach minimum values (zero for a negative

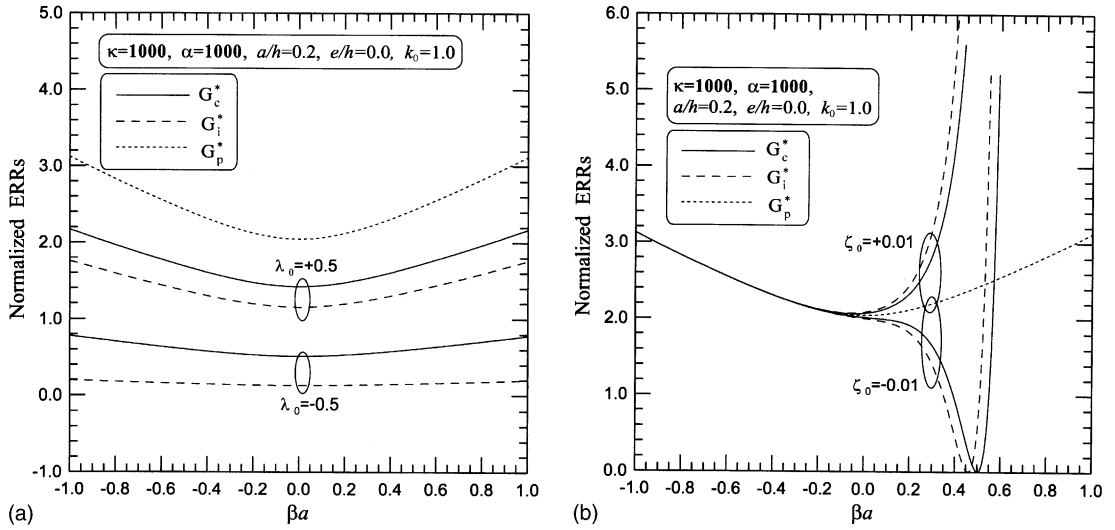

Fig. 7. Normalized ERRs versus βa in a center cracked piezoelectric strip: (a) constant electric displacement; (b) constant electric field.

electric field and a certain value corresponding to $\beta a = 0$ for a positive electric field), after then sharply increase with the increase of βa. It can be also seen that the effects of the electric crack surface assumptions are negligible in the zone of negative βa except in the vicinity of $\beta a \approx 0$.

The influence of the crack length on the ERRs is shown in Fig. 8(a) and (b). All the electrical crack conditions cast the same trends, i.e. the ERRs increase as a/h increases. The traditional approaches have the same ERRs no matter what the electric field is positive or negative, because the permeable solution is independent of the electric load as well as the impermeable solution have the symmetry with respect to $\zeta_0 = 0$ as can be seen in Fig. 6.

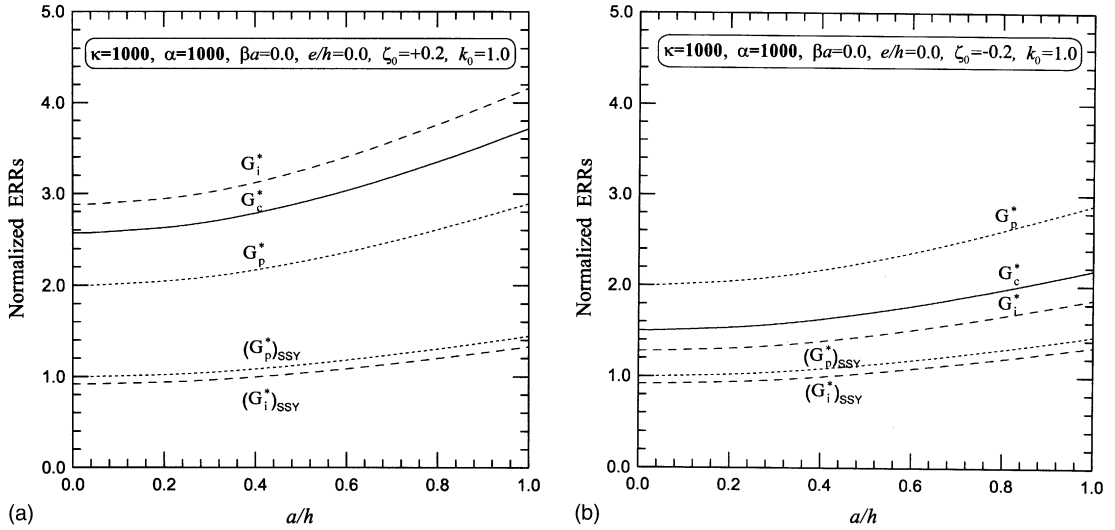

Fig. 8. Normalized ERRs versus a/h in a center cracked piezoelectric strip: (a) positive electric field ($\lambda_0 = 1.4$, $\zeta_0 = +0.2$); (b) negative electric field ($\lambda_0 = 0.6$, $\zeta_0 = -0.2$).

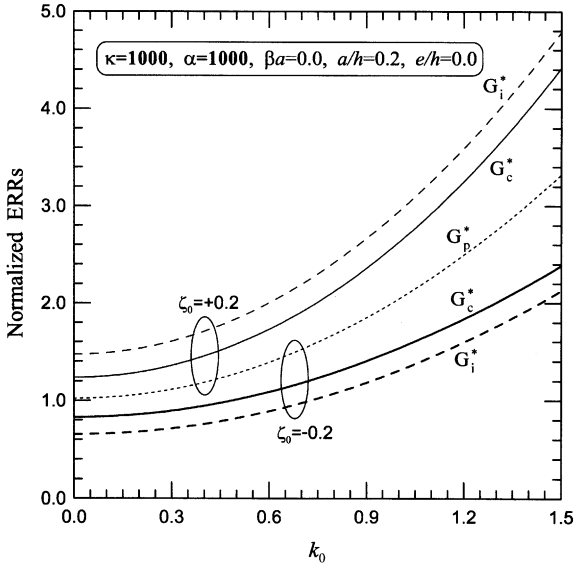

Fig. 9. Normalized ERRs versus k_0 in a center cracked piezoelectric strip.

In Fig. 9, the effect of the EMCC k_0 on the ERRs is shown. It reveals that the ERRs increase regardless of the direction of electric loads as the EMCC increases. Here the ERRs when $k_0 = 0$ represent the solutions of the isotropic dielectric. This is useful for illustrating the issues of purely elastic materials which must be addressed if cracks in piezoelectrics are to be understood.

Fig. 10 displays the normalized ERRs versus the crack position in a piezoelectric strip. The ERRs increase with the increase of e/h.

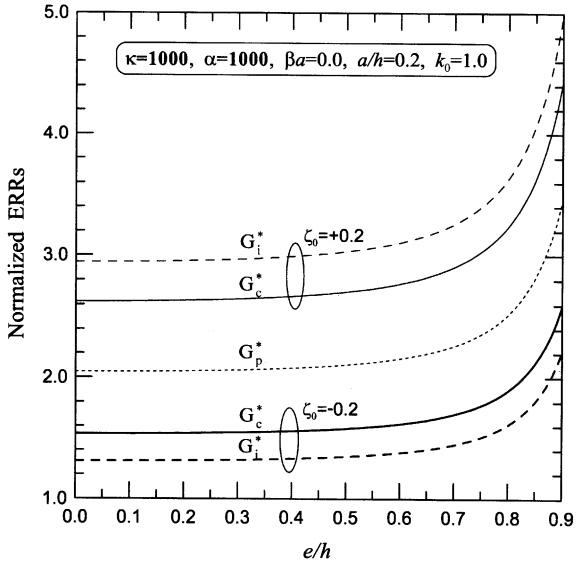

Fig. 10. Normalized ERRs versus e/h in a cracked piezoelectric strip.

Finally, we consider the effect of the electrically yielded zone size ω_s/a upon the ECCP and the electric loads. For the brevity of the computation, we consider a homogeneous infinite piezoelectric material (i.e. $h \to \infty$ and $\beta = 0$). Then, the normalized strip length ω_s/a is determined from Eq. (60) as

$$\frac{\omega_s}{a} = \sec\left[\frac{\pi}{2}\frac{D_0}{D_s}(1 - D_r)\right] - 1. \tag{85}$$

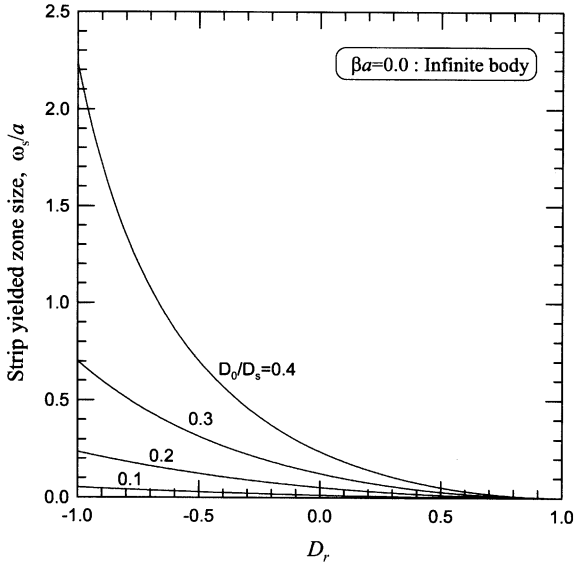

Fig. 11. Normalized strip yielded zone size ω_s/a versus D_r in a cracked infinite piezoelectric material.

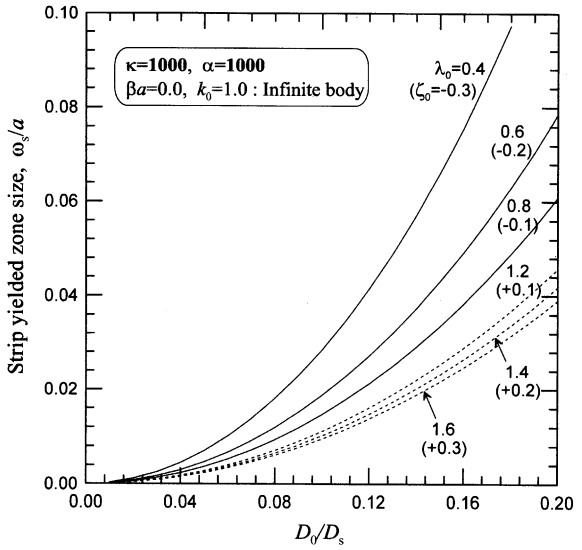

Fig. 12. Normalized strip yielded zone size ω_s/a versus D_0/D_s with the variation of electric loads in a cracked infinite piezoelectric material.

Fig. 11 shows the dependence of D_r with the variation of D_0/D_s on the ω_s/a. The longer size of strip yielded zone is observed in the interval of negative ECCP ($\lambda_0 < k_0^2$) and higher applied electric displacements.

Fig. 12 displays the dependence of D_0/D_s with the variations of electric loads λ_0 and ζ_0 on the ω_s/a in an ellipsoidal flaw of $\kappa = 1000$ and $\alpha = 1000$. It shows that ω_s/a increases as D_0/D_s increases with the decrease of λ_0. The decrease of λ_0 means that the piezoelectric materials are electrically more ductile; the plastic yielding zone ahead of the crack tip is much smaller than the electric saturation zone. However, the effect of ζ_0 is different that of λ_0, that is, the electric ductility, resistance to fracture, increases as the negative electric field prevails.

6. Conclusions

Motivated by recent researches on the role of the electrical polarization saturation in crack growth of ferroelectric/piezoelectric materials, the electrically nonlinear crack problem in a functionally graded piezoelectric ceramic strip has been analyzed by the integral transform approach. The analysis has been conducted on the unified crack boundary condition to describe more realistic cracks. The intensity factors and ERRs have been obtained via auxiliary functions determined from Fredholm integral equations.

It is observed that the ERRs based on the unified crack boundary condition is always positive and falls between those obtained from the impermeable crack and permeable crack. It is also found that the ERRs are dependent on the ECCP with two ellipsoidal crack parameters, the direction and magnitude of electrical loads, the material gradation, the crack length, the EMCC and the crack location.

Since the concept of electrical polarization saturation in associated with the electrically unified crack assumption gives a plausible explanation for some discrepancies between experiments and linear piezoelectric model, it is expected to play an essential role for a physically more realistic description of fracture behaviors in piezoelectric ceramics.

Acknowledgements

The author is very grateful to two reviewers for their helpful comments and suggestions.

References

Bleustein, J.L., 1968. A new surface wave in piezoelectric materials. Applied Physics Letters 13, 412–413.

Chen, J., Liu, Z.X., Zou, Z.Z., 2003a. Electromechanical impact of a crack in a functionally graded piezoelectric medium. Theoretical and Applied Fracture Mechanics 39, 47–60.

Chen, J., Liu, Z.X., Zou, Z.Z., 2003b. Dynamic response of a crack in a functionally graded interface of two dissimilar piezoelectric half-planes. Archive of Applied Mechanics 72, 686–696.

Cherrepanov, G.P., 1979. Mechanics of Brittle Fracture. McGraw-Hill, New York. pp. 317–341.

Copson, E.T., 1961. On certain dual integral equations. Proceedings of the Glasgow Mathematical Association 5, 19–24.

Fulton, C.C., Gao, H.J., 1997. Electrical nonlinearity in fracture of piezoelectric ceramics. Applied Mechanics Review 50, S56–S63.

Gao, H.J., Barnett, D.M., 1996. An invariance property of local energy release rates in a strip saturation model of piezoelectric fracture. International Journal of Fracture 79, R25–R29.

Gao, H., Zhang, T.-Y., Tong, P., 1997. Local and global energy release rates for an electrically yielded crack in a piezoelectric ceramic. Journal of the Mechanics and Physics of Solids 45, 491–510.

Gong, X., Suo, Z., 1996. Reliability of ceramic multilayer actuators: a nonlinear finite element simulation. Journal of the Mechanics and Physics of Solids 44, 751–769.

Han, X., Wang, T., 1999. Interacting multiple cracks in piezoelectric materials. International Journal of Solids and Structures 36, 4183–4202.

Hao, T.H., Gong, X., Suo, Z., 1996. Fracture mechanics of the design of ceramic multilayer actuators. Journal of the Mechanics and Physics of Solids 44, 23–48.

Jin, Z.-H., Batra, R.C., 1996. Some basic fracture mechanics concepts in functionally graded materials. Journal of the Mechanics and Physics of Solids 44, 1221–1235.

Jin, B., Zhong, Z., 2002. A moving mode-III crack in functionally graded piezoelectric material: permeable problem. Mechanics Research Communications 29, 217–224.

Kwon, S.M., Lee, J.S., Lee, K.Y., 2002a. Moving eccentric crack in a piezoelectric strip bonded to elastic half planes. International Journal of Solids and Structures 39, 4395–4406.

Kwon, S.M., Son, M.S., Lee, K.Y., 2002b. Transient behavior in a cracked piezoelectric layered composite: anti-plane problem. Mechanics of Materials 34, 593–603.

Lynch, C.S., Yang, W., Collier, L., Suo, Z., McMeeking, R.M., 1995. Electric field induced cracking in ferroelectric ceramics. Ferroelectrics 166, 11–30.

McMeeking, R.M., 1999. Crack tip energy release rate for a piezoelectric compact tension specimen. Engineering Fracture Mechanics 64, 217–244.

Park, S.B., Sun, C.T., 1995. Fracture criteria for piezoelectric ceramics. Journal of American Ceramic Society 78, 1475–1480.

Ru, C.Q., 1999. Effect of electrical polarization saturation on stress intensity factors in a piezoelectric ceramic. International Journal of Solids and Structures 36, 869–883.

Ru, C.Q., Mao, X., 1999. Conducting cracks in a piezoelectric ceramic of limited electrical polarization. Journal of the Mechanics and Physics of Solids 47, 2125–2146.

Ru, C.Q., Mao, X., Epstein, M., 1998. Electric-field induced interfacial cracking in multilayer electrostrictive actuators. Journal of the Mechanics and Physics of Solids 46, 1301–1318.

Shen, S., Nishioka, T., Kuang, Z.-B., Liu, Z., 2000. Nonlinear electromechanical interfacial fracture for piezoelectric materials. Mechanics of Materials 32, 57–64.

Wang, B.L., 2003. A mode III crack in functionally graded piezoelectric materials. Mechanics Research Communications 30, 151–159.

Wang, T.C., 2000. Analysis of strip electric saturation model of crack problem in piezoelectric materials. International Journal of Solids and Structures 37, 6031–6049.

Wang, B.L., Mai, Y.-W., 2003. On the electrical boundary conditions on the crack surfaces in piezoelectric ceramics. International Journal of Engineering Science 41, 633–652.

Xu, X.L., Rajapakse, R.K.N.D., 2001. On a plane crack in piezoelectric solids. International Journal of Solids and Structures 38, 7643–7658.

Yamada, K., Sakamura, J., Nakamura, K., 2000. Equivalent network representation for thickness vibration modes in piezoelectric plates with an exponentially graded parameter. Japanese Journal of Applied Physics 39, L34–L37.

Yang, W., Suo, Z., 1994. Cracking in ceramic actuators caused by electrostriction. Journal of the Mechanics and Physics of Solids 42, 649–663.

Zhang, T.-Y., Tong, P., 1996. Fracture mechanics for mode III crack in a piezoelectric material. International Journal of Solids and Structures 33, 343–359.

Zhao, M.H., Shen, Y.P., Liu, G.N., Liu, Y.J., 1999. Dugdale model solutions for a penny-shaped crack in three-dimensional transversely isotropic piezoelectric media by boundary-integral equation method. Engineering Analysis with Boundary Elements 23, 573–576.